88 KACC 1988.10.21~22

Stability of the Robot Compliant Motion Control, Part II : Implementation

Sungkwun Kim

Samsung Semiconductor and
Telecommunications Co., Ltd.

Abstract: We have shown how unstructured modeling was used to derive a general stability condition in Part 1. In Part 2, we focus on the particular dynamics (structured modeling) of the robot manipulator and environment. Using rigid body dynamics, the stability condition for the direct drive robots has been achieved in terms of the Jacobian and robot tracking controller. Combining the structured and unstructured modeling, a stability condition for a particular application can be obtained. This approach has been used to analyze compliant motion on the University of Minnesota robot using a feedforward torque controller. We have obtained a stability condition for this application. Through both simulation and experiment, the sufficiency of this condition has been demonstrated. For a sufficient stability condition, recall that if the condition is satisfied, then the stability is guaranteed; however, if the condition is violated, no conclusion can be made.

1. Introduction

In part 1, a general stability condition for constrained maneuvers was derived using the unstructured model of a robot and its environment. It allows us to understand the fundamental concept in stability when a robot interacts with an environment. However, this approach may not lead to any design procedure because of the unstructured model. For realizing the fundamental stability concept, in this Part, the stabilty condition is extended for a structured model. The structured model for the compliance control with the feedforward position controller is derived [Kazerooni and Kim, 1988b]. The sensitivity function of the system is derived from the structured model. The stability condition for the feedforward controller is expressed a function of Jacobian and robot feedback loop gain. The compliant motion controller modelled is simulated and implemented on the University of Minnesota Robot.

2. Structured Model for Compliant Motion Control

To evaluate the nonlinear stability condition, a compliance controller was implemented on the University of Minnesota robot, a statically-balanced, direct-drive, three degree of freedom robot which was constructed to evaluate nonlinear, compliance control algorithms (Kazerooni, Kim, 1987a,b, 1988a,b) The detailed compliant motion control scheme is proposed as in Figure 1. In the block diagram in Figure 1, the position controller is the same as the feedforward controller in Chapter 6. kin() represents the forward kinematic equation. y is 3 x 1 vector of the actual position of the end point of a robot at the global coordinate, and x_o is the initial position vector of the point of contact before deformation occurs. E is the environment dynamics. f is 3 x 1 vector of the forces applied to the global coordinate. J^{-1} and J^T are the inverse and the transpose of the Jacobian with respect to the global coordinate. H is the compensator to be designed. Δx is the resultant deflection from mapping f using the compensator H. $\Delta\theta$ is n x 1 vector of the angular deflection in joint space mapped from Δx. Note that J^{-1} and J^T are required on line computation. $M(\theta)$ is the inertia matrix of a robot, and $C(\theta,\dot{\theta})$ is the vector of the centrifugal, Coriolis, gravity, and frictional forces. $\hat{M}(\theta_d)$ and $\hat{C}(\theta_d,\dot{\theta}_d)$ are the estimates of $M(\theta)$ and $C(\theta,\dot{\theta})$, respectively. $\ddot{\theta}$, $\dot{\theta}$, and θ are the measured accelerations, veloc-

ities, and positions, respectively. $\ddot{\theta}_d$, $\dot{\theta}_d$, and θ_d are the desired accelerations, velocities, and

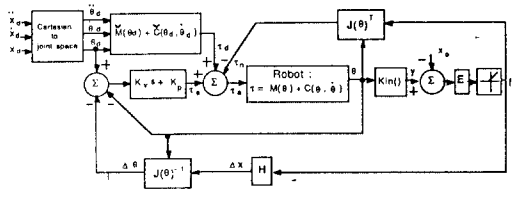

Figure 1 Detailed compliant motion control scheme using impedance control method

positions, respectively, K_p and K_v are diagonal matrics containing the position and velocity gains in the controller.

From the block diagram, the actual torque, τ_a, to the robot is given by

$$\tau_a = \tau_d + \tau_e - \tau_n \qquad (1)$$

where τ_d is the desired torque to generate the trajectory of a robot, τ_e is the compensated torque resulting from the position and velocity error loops and the foece compensator loop. τ_n is the natural feedback torque when the robot is in contact with and environment.

Thus, the actual torque from Figure 1 can be rewritten by

$$\tau_a = \hat{M}(\theta_d)\ddot{\theta}_d + \hat{C}(\theta_d, \dot{\theta}_d) + k_v(\dot{\theta}_d - \dot{\theta}) + k_p(\theta_d - \theta) - (k_v \Delta\dot{\theta} + k_p \Delta\theta) - J^T f \qquad (2)$$

where

$$f = E(y - x_o) \qquad (3)$$

$$y = kin(\theta) \qquad (4)$$

$$= J^{-1}(\theta)\, Hf \qquad (5)$$

The actual robot dynamics are also expressed as in equation (6).

$$\tau = M(\theta)\ddot{\theta} + C(\theta, \dot{\theta}) \qquad (6)$$

Combining (2) and (6) results in

$$M(\theta)\ddot{\theta} = \hat{M}(\theta_d)\ddot{\theta}_d + \hat{C}(\theta_d, \dot{\theta}_d) + k_v(\dot{\theta}_d - \dot{\theta}) + k_p(\theta_d - \theta) - (k_v \Delta\dot{\theta} + k_p \Delta\theta) - J^T f - C(\theta, \dot{\theta}) \qquad (7)$$

Since $M(\theta) \approx \hat{M}(\theta_d)$, $\hat{C}(\theta_d, \dot{\theta}_d) \approx C(\theta, \dot{\theta})$ in the feedforward controller, equation(7) can be simplified as in equation(8)

$$\ddot{\theta} = \ddot{\theta}_d + \hat{M}(\theta_d)^{-1}[k_v(\dot{\theta}_d - \dot{\theta}) + k_p(\theta_d - \theta) - (k_v \Delta\dot{\theta} + k_p \Delta\theta) - J^T f] \qquad (8)$$

Equation(8) is the nonlinear inpedance control algorithm with a feedforward position controller. Note that the last term in equation(8) results from a natural feedback loop.

3. Stability Condition for Feedforward Controller

In order to find a stability bound on H, we must determine the operator, V: $e(t) \longrightarrow f(t)$, for the robot controller. To determine the greatest bound on V, we assume that the wall is very stiff, such that $y \approx xo$. In this case, one can find the sensitivity of the robot from equation(8) to calculate α_4. The sensitivity is the inverse of the stiffness. The stiffness of a manipulator is the ratio of the static force applied at the end point of the manipulator to the resultant static deflection at the same point. The stiffness is determined by the feedback loop gains of individual joint actuators as well as the mechanical construction of the manipulator.

In this analysis we assume that the effects of both the joint mechanical compliancy and link flexibility can be neglected.

To derive the sensitivity of the system with a feedforward torque controller as in Figure 1, equation (8) can be rewritten as in equation (9)

$$M\ddot{\theta}_c + k_v\dot{\theta}_c + k_p\theta_c - J^T f = 0 \qquad (9)$$

where $\theta_c = \theta_d - \theta$. Note that the angular deflection, $\Delta\theta$, resulting from the force feedback control loop is neglected.

From equation(9), a steady state case is considered to obtain the sensitivity of the manipulator, the joint deflection, θ_c, of the manipulator is derived

$$\theta_c = k_p^{-1} J^T f \qquad (10)$$

The end point deflection, x_c, at the Cartesian coordinate for a given point is obtained by

$$x_c = J\theta_c \tag{11}$$

To find the sensitivity of the manipulator at the Cartesian space, substituting equation (10) into equation(11) reaults in

$$x_c = J k_p^{-1} J^T f \tag{12}$$

which can be represented as

$$x_c = S f \tag{13}$$

where $$S = J k_p^{-1} J^T \tag{14}$$

Thus, the sensitivity, S, varies with the manipulator configuration, since the Jacobian is a function of the configuration.

To find V, equation(13) can be rewritten as

$$f = S^{-1} x_c \tag{15}$$

or

$$f = (J^{-T} k_p J^{-1}) x_c \tag{16}$$

Therefore, V is the inverse of the sensitivity and is given by

$$V = J^{-T} k_p J^{-1} \tag{17}$$

Using inequality (18) in Part 1, the stability condition is:

$$\gamma < \frac{1}{\alpha_4} \tag{18}$$

where α_4 is the supremum of $\sigma_{max}(J^{-T} k_p J^{-1})$ over the commanded trajectory. Equivalently one can satisfy inequality (19)

$$\gamma < \text{infimum of } \sigma_{min}(J k_p^{-1} J^T) \text{ over the commanded trajectory} \tag{19}$$

One must calculate the minimum singular value of $(J k_p^{-1} J^T)$ at each point in the commanded trajectory. The infimum is the lowest of all the minimum singular values. The gain of H (expressed in terms γ) must be chosen smaller than this infimum. From inequality (19), the stability region will approach zero when the robot maneuvers near a singular point (det(J)$\longrightarrow$ o) and/or when the position gains approach infinity. Both cases are instances of "infinite stiffness" for the robot, the first is due to the robot configuration, while the second is due to the tracking controller.

The static joint stiffnesses of the manipulator used for the compliance control were 315Nm/rad for joint 1, 481 Nm/rad for joint 2, 111 Nm/rad for joint 3.

4. Experimental Setup

In order to examine the behavior of the proposed compliant motion controller, experiments have been conducted. The experimental set up in shown as in Figure 2. A three dimensional force sensor (Kistler, type 9251 A) is mounted at the wrist at the manipulator to measure the forces at the wrist coordinate. The end effector has a hemispherical shape (radius : 45 .7mm; weight: 0.4kg) made of aluminium alloy 2024 T6 to avoid moment force applied to the force sensor. The surface of the end effector was hard coated[1] to reduce friction and increase abrasion resistance. An aluminium alloy wall is used as an environment and is located 0.53m from the origin of the robot global coordinate as shown in Figure 2. Motor 2 was mechanically locked while motors 1 and 3 were used to actuate the robot for horizontal maneuvering; this resulted in planar, horizontal motion of the robot end point in global, Cartesian space. The reference trajectory in the experiment as shown in Figure 3 is an arc(Radius= 0.565m). The linear speed of the end effector is 0.42m/sec.

Considerable high frequency noise in the force sensor output was observed in excess of 200 Hz. To eliminate this effect, the signal from the force sensor was passed through a low pass filter. If the sampled signal has frequency components higher than sampling frequency, aliasing can produce unwanted noise on the sensed force. To reduce aliasing noise, low pass filters, which have cut off frequencies of 70Hz, were used to cut off at less than one half the salpming frequency. The sampling rate of the force sensor is 147Hz(6.8m sec).

Since the experiments are all two-dimensional, H is a 2x2 matrix operating on contract forces which are normal tangential to the wall. (The end point force measurements were resolved into the

global coordinate frame .) In these experiments, only the compliancy in the direction normal to the wall was supplemented, so the following from of H was chosen:

$$H = \begin{bmatrix} \frac{H_0}{\tau_h s+1} & 0 \\ 0 & 0 \end{bmatrix} \qquad (20)$$

where τ_h is empirically chosen constant used to filter the high frequency noise in the force measurement. τ_h was fixed at 0.05 for all the experiments. The function, r(t), shown in Figure 3 by the dashed line, is chosen as the assigned trajectory to the robot. Since H has only one non-zero member, then γ will be the maximum value of the magnitude of $H_0/(\tau_h j\omega + 1)$. The maximum value of H is H_0 and occurs at DC $(\omega=0)$.

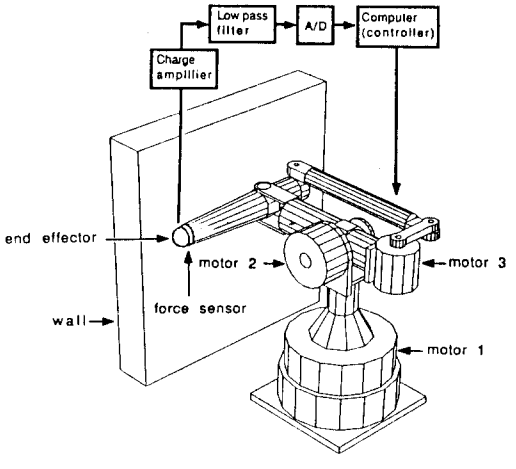

Figure 2 Experimental set up

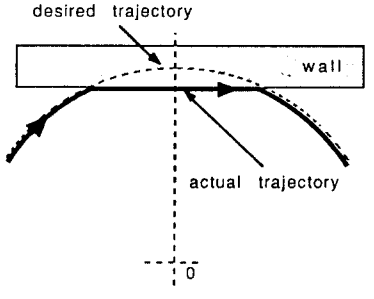

Figure 3 Trajectory of the end effector: actual path is heavy line; velocity is 0.42 m/sec

5. Experimental and Simulation Results

5.1 Simulation

The compliant motion controller in the previous section was simulated using the mathematical model in equation (8). In order to realize the simulation of the model in equation(8), the following assumptions have been made:

(1) The effects of both the robot joint mechanical compliancy and link flexibility can be neglected. (The manipulator links are modelled as rigid bosies)

(2) The wrist force sensor dynamics are neglected in the dynamic model.

(3) The actuator dynamics are also neglected. The actuators are only torque sources.

(4) The environment(wall) dynamics are modelled as a spring, the surface of the environment is somooth, and the coefficient of the friction on the wall is 0.4.

With these assumptions, the model in equation(8) was used to simulate the system. The nonlinear differential equations were solved by the Runge-Kutta fourth order integration method. In order for the numerical solution to be stable, the integration time step used in the simulation was 0.1m sec. The robot sampling time of 6.8m sec was used. For the natural feedback loop, the torque τ_n was computed for every integration time, the other torques controlled by the robot controller were updated every sampling time.

The reference trajectory and the speed at the end effector of the manipulator were the same as those in experimental setup. The position gains used were 315 Nm/rad for joint 1,481 Nm/rad for joint2, and 111 Nm/rad for joint3. The velocity gains used were 35N-sec/rad for joint 1,35N-sec/rad for joint 2, and 13,1 N-sec/rad for joint 3 that include the damping resulting from its mechanical system. The environment stiffness was chosen as 80000m/N so that the impulsive force due to the collision was the same magnitude as that in the experimental thst.

To choose the compensator gain, H, the static sensitivity, S, of the manipulator was calculated using the equations in Section 3 for the given trajectory in the experimental setup. The minimum and maximum singular value of the sensitivity are about 0.00032m/N and 0.002lm/N, respectively as shown in Figure 4. The compecsator gains tested

were 0, 0.0003, 0.0005, and 0.0015. H_0=0 and 0.0003 were chosen to teat the $H_o < \sigma_{min}(S)$ stability condition, and H_o = 0.0005 and 0.0015 were chosen for $\sigma_{min}(S) < H_o < \sigma_{max}$ condition.

The results of the simulation will be presented in next section with the experimental results.

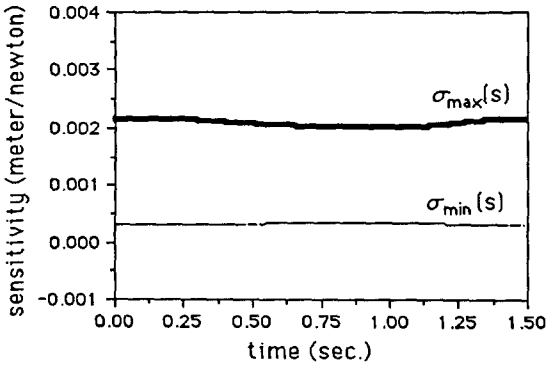

Figure 4 The maximum amd minimum singular values of the sensitivity function for the actual trajectory shown in Figure 3.

5.2 Experimental and Simulation Results

The stability criterion for compliance motion control discussed in the previous sections has been investigated by simulation and experiments on the University of Minnesota Robot. The results of the computer simulation are similar to the experimental results as shown in Figure 5 through 8.

Figure 5 and 6 shown the actual performance of the compliant motion controller on the aluminium wall surface for a given constant speed. The compensator gains used were 0.0 and 0.0003 for the normal direction to the wall, and 0 for the tangential direction. Figure 5 shows the contact force against time when H_o=0. Figure 6 shows the contact force against time when H_o=0.0003. Upon contacting the wall, the end effector slides along a chord of the radius defined by the surface of the wall as shown in Figure 3. At the moment of contact with the wall there is an impulsive force due to the collision of the end effector with the rigid surface, but immediately afterward the force drops to zero. The apparently random fluctuations are due to noise in the system. The difference between the actual position and desired position results in a contact force determined by the target impedance. Both figures show that the system remains stable in the constrained motion when $H_o < \sigma_{min}(J k_p^{-1} J^T)$. The co contact force when H_o=0.0003 is reduced about 20% in comparison to that when H_o=0.

Figure 7 shows the performance of the system when H_o=0.0005. The system still remains stable in the constrained motion, even though H is chosen slightly larger than $\sigma_{min}(J k_p^{-1} J^T)$. The contact force is reduced about 30% of that when H_o=0. Figure 8 shows that the system is unstable in the constrained motion when H_o=0.0015 that exceeded the lower bound on $\sigma_{min}(J k_p^{-1} J^T)$; hence, the stability condition was been violated. There is a discrepancy between the experimental and simulation results because the effects of the mechanical compliancy of the robot and the environment deformation were not included in the simulation. These effects are highly nonlinear and difficult to model because of a lack of knowledge concerning the exact dynamic behavior. For previous results, this simplification did not significantly affect the system. However, for for H_o=0.0015 these effects dominate the performance of controller, explaining the discrepancy.

Figure 9 shows the actual performance of the controller on the rubber surface (0.5cm thickness) secured to the aluminium wall. The experimental conditions are the same as on the isolated aluminium surface. It shows that the system is more stable when a compliance element is placed between the robot and its environment.

Through those simulation and experiments, the stability criterion in equation(18) has been verified. The stability criterion, $H < \sigma_{min}(S)$, is a sufficient condition, but not necessary.

Comparing with the figures mentioned above, it is quite clear that the compliant motion control scheme using impedance cotrol method shows good control of the interface force during contact task when the compensator gain is properly chosen by the stability criterion. Thus, this controller can be used for both constrained and unconstrained maneuverings. As expected, the robot becomes more stable when it makes contact with a rubber surface than with the stiff aluminum surface. The experimental results also show that with an appropriately designed mechanism, stable interaction may be achieved without using force feedback. The appropri-

ately designed mechanism yields a substantial improvement in contact task performance.

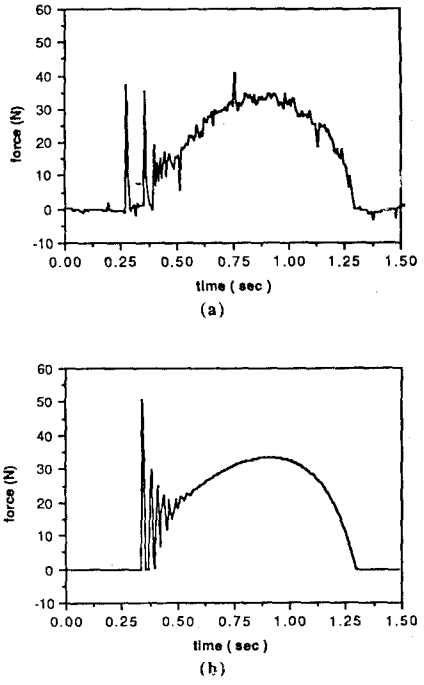

Figure 5 Normal contact force on the aluminum surface vs. time. H_o=0 satisfies the stability condition. (a) experiment; (b) simulation

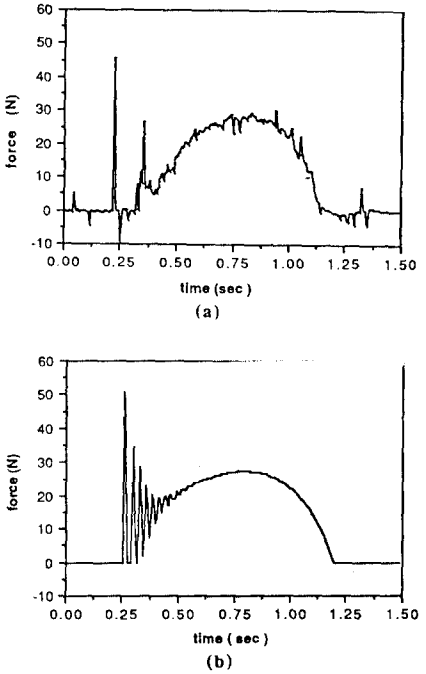

Figure6 Normal contact force on the aluminum surface vs. time. H_o=0.0003 satisfies the stability condition . (a) experiment; (b) simulation

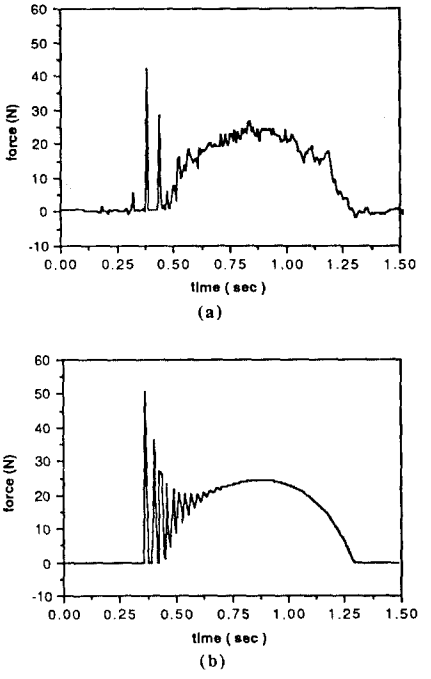

Figure7 Normal contact force on the aluminum surface vs. time. H_o=0.0005 violates the stability condition, however the system is stable. (a)experiment; (b) simulation

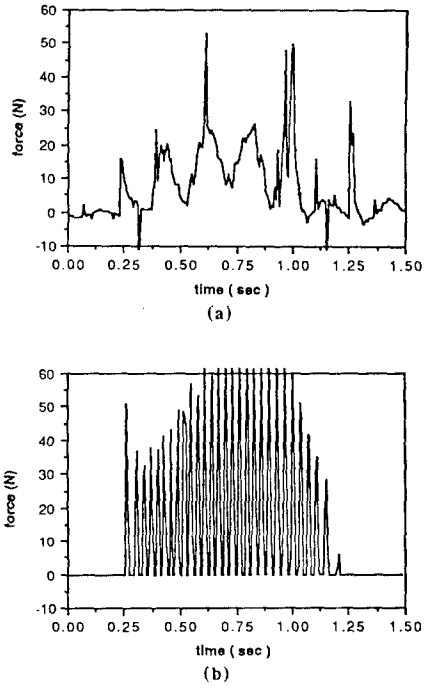

Figure8 Normal contact force on the aluminum surface vs. time. H_o=0.0015 does not satisfy the stability condition. (a) experiment; (b) simulation

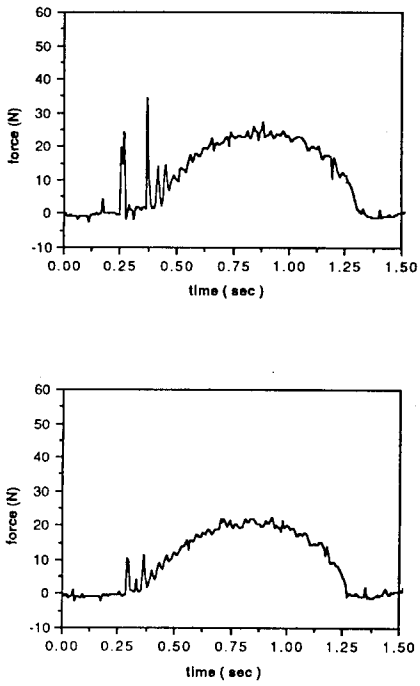

Figure 9 Normal contact force on the rubber surface (thickness: 0.5mm) on the aluminum wall. (a)H_o=0; (b) H_o=0.0005

6. Summary

We have shown how unstructured and structured modeling can be combined to derive a stability condition for a particular robot performing compliant motion. The unstructured modeling, which focuses on the input-output characteristics of the system, enables the derivation of a general stability condition. The structured modeling contains the robot and environment dynamics which are specific to a particular robot and controller architecture. Combining the structured and unstructured modeling, a stability condition for a particular application can be obtained. We have used this approach to analyze compliant motion on the University of Minnesota robot using a feedforward torque controller. We have obtained a stability condition for this application. Through both simulation and experiment, the sufficiency of this condition has been demonstrated. We have shown that for the stability of the environment and the robot taken as a whole. there must be some initial compliancy either in the robot or in the environment. The major results of this research may be summarized as follows:

(1) The stability criterion $\mathbf{H < \sigma_{min}(S)}$, based on the unstructured model for the robot and its environment is a sufficient condition. not necessary. Note that the stability condition for the structuted model is $\mathbf{H < \sigma_{min}(J\, k_p^{-1}\, J^T)}$.

(2) As expected, the robot becomes more stable when in makes contact with a rubber surface than with the stiff aluminum surface.

(3) These experimental results clearly demonstrated that the impedance control is a practical strategy for both constrained and unconstrained tasks.

(4) The experimental results also showed that with an appropriately designed mechanism, stable interaction may be achieved without using force feedback(large robot sensitivity). The appropriately designed mechanism yields a substantial improvement in contact task performance.

Acknowledgment

This paper describes research done at the Motion Control Laboratory of the University of Minnesota with financial support from the Productivity Center and the Graduate School.

The Author wishes to thank Dr. Taiyoung Ahn for preparing this manuscript.

References

Kazerooni, H., and Kim, S., 1987a, "Design and Construction of a Statically-Balanced Direct Drive Arm", ASME Advanced Design Automation Conference, Volume 2, Boston, MA, September 1987, pp. 17-23.

Kazerooni, H., and Kim, S., 1987b, "Statically-Balanced Direct Drive Robot for Compliance Control Analysis", ASME Winter Annual Meeting, in "Modeling and Control of Robotic Manipulators and Manufacturing Process", DSC - Volume 6, Boston, MA., December 1987, pp. 193-201.

Kazerooni, H., and Kim, S., 1988a, "A New Architecture for Direct Drive Robots", IEEE International Conference on Rocotics and Automation, Volume 1, Philadelphia, PA, April 1988, pp.442-445

Kazerooni, H., and Kim, S., 1988b, "Design and Control of a Statically Balanced Direct Drive Manipulator", USA-JAPAN Symposium on Flexible Automation, Volume 1, Minneapolis, Minnesota, July 1988, pp. 449-454.